Rocks, water, and noble liquids: Unfolding the flavor contents of supernova neutrinos

Sebastian Baum,[1,*] Francesco Capozzi,[2,3,†] and Shunsaku Horiuchi[2,4,‡]

[1]*Stanford Institute for Theoretical Physics, Stanford University, Stanford, California 94305, USA*
[2]*Center for Neutrino Physics, Department of Physics, Virginia Tech, Blacksburg, Virginia 24061, USA*
[3]*Instituto de Física Corpuscular, Universidad de Valencia & CSIC, Edificio Institutos de Investigación, Calle Catedrático José Beltrán 2, 46980 Paterna, Spain*
[4]*Kavli IPMU (WPI), UTIAS, The University of Tokyo, Kashiwa, Chiba 277-8583, Japan*

(Received 5 April 2022; accepted 11 October 2022; published 9 December 2022)

Measuring core-collapse supernova neutrinos, both from individual supernovae within the Milky Way and from past core collapses throughout the Universe (the diffuse supernova neutrino background, or DSNB), is one of the main goals of current and next generation neutrino experiments. Detecting the heavy-lepton flavor (muon and tau types, collectively ν_x) component of the flux is particularly challenging due to small statistics and large backgrounds. While the next galactic neutrino burst will be observed in a plethora of neutrino channels, allowing us to measure a small number of ν_x events, only upper limits are anticipated for the diffuse ν_x flux even after decades of data taking with conventional detectors. However, paleo detectors could measure the time-integrated flux of neutrinos from galactic core-collapse supernovae via flavor-blind neutral current interactions. In this work, we show how combining a measurement of the average galactic core-collapse supernova flux with paleo detectors and measurements of the DSNB electron-type neutrino fluxes with the next-generation water Cherenkov detector Hyper-Kamiokande and the liquid noble gas detector DUNE will allow to determine the mean supernova ν_x flux parameters with precision of order ten percent. Realizing this potential requires both the cosmic supernova rate out to $z \sim 1$ and the integrated Galactic supernova rate over the last $\sim$1 Gyr to be established at the $\sim$10% level.

DOI: 10.1103/PhysRevD.106.123008

I. INTRODUCTION

Supernovae play an important role for the workings of our Universe as well as for our understanding thereof. The rapid injection of energy from supernovae is crucial for the properties of galaxies, and the extreme environment of a supernova makes them the birthplaces of much of the heavy elements in our Universe as well as prolific sources of energetic cosmic rays. Neutrinos play a crucial role in the explosion mechanisms of supernovae, not least because the matter density during the initial stages of a core-collapse supernova is so high that neutrinos are the only (known) particles which can escape this environment. While core-collapse supernovae produce enormous fluxes of all flavors of neutrinos, to date, the only supernova neutrinos measured by terrestrial experiments are the historical $\bar{\nu}_e$ events detected from SN1987A [1–4]. Detecting all flavors of supernova neutrinos is an important goal, for example to infer the total energetics of the collapse, to test complex neutrino oscillation phenomena, and to search for physics beyond the Standard Model [5].

In the upcoming decades, the next generation of neutrino detectors, in particular Hyper-Kamiokande [6] and DUNE [7], will provide unprecedented sensitivity to supernova neutrinos. Utilizing charged-current interactions, Hyper-Kamiokande is predominantly sensitive to $\bar{\nu}_e$ neutrinos while DUNE is mostly sensitive to the ν_e fluxes. In order to detect heavy lepton flavor neutrinos $\nu_x = \{\nu_\mu, \bar{\nu}_\mu, \nu_\tau, \bar{\nu}_\tau\}$, one must rely on processes with significantly smaller event rates. One strategy to detect ν_x is to use scattering on protons in scintillator detectors [8–12]. Another strategy is to exploit flavor-blind channels, for example, elastic scattering events in large direct dark matter detection experiments, and subtract the (anti-)electron-type neutrino contribution by merging datasets.

If next-generation neutrino detectors are operational at the time of the next galactic core-collapse event, supernova neutrinos of all flavors will be measured with relatively large statistics—Hyper-Kamiokande, DUNE and JUNO, would detect $\mathcal{O}(10^5)\,\bar{\nu}_e$, $\mathcal{O}(10^3)\,\nu_e$ and $\mathcal{O}(10^2)\,\nu_x$ events, respectively. In addition, the current generation of tonne-scale dark matter detectors such as XENONnT, LZ, or PandaX-4T, would make flavor-blind detections of neutrinos from such a galactic core-collapse event [13,14]. While neutrinos from the next galactic core-collapse supernova will teach us invaluable lessons about neutrinos and

*sbaum@stanford.edu
†fcapozzi@ific.uv.es
‡horiuchi@vt.edu

supernova physics, this approach also comes with drawbacks: The galactic core-collapse supernova rate is estimated to be 2–3 per century [15–20] and the only remedy is patience. Furthermore, one would measure the neutrinos from an individual core-collapse supernova which may well be atypical. Both of these issues are mitigated by attempting to detect neutrinos from the diffuse supernova neutrino background (DSNB), the neutrino flux from distant core-collapse supernovae throughout the Universe [21,22]. However, detecting the DSNB is challenging due to its relatively small neutrino flux and because the DSNB spectrum is significantly redshifted—the DSNB flux is dominated by supernovae at redshifts $z \sim 1-2$. The next generation of neutrino detectors, in particular Hyper-Kamiokande and DUNE, are expected to detect $\bar{\nu}_e$ and ν_e neutrinos from the DSNB and measure the corresponding neutrino flux parameters. However, no (conventional) neutral-current detector with the required combination of exposure and energy threshold is available to measure the ν_x fluxes. Even future direct dark matter detectors such as DARWIN [23] are expected to set only upper limits on the DSNB ν_x flux roughly an order of magnitude above the expected flux [24].

In this work, we show the prospects of *paleo detectors* to measure the ν_x supernova neutrino flux. Rather than operating a real-time laboratory experiment to search for neutrinos, paleo detectors [25–27] would use nuclear damage tracks recorded in natural minerals of geological ages (100 Myr − 1 Gyr) to search for neutrino-induced nuclear recoils [28]. Many minerals are excellent solid state track detectors [29–32] and retain the damage tracks caused by nuclear recoils for timescales which can exceed the age of the Earth by many orders of magnitude. Modern microscopy techniques such as small angle x-ray scattering [33–35] potentially allow for the readout of these damage tracks in macroscopic samples. Paleo detectors have been considered to study atmospheric [36] and solar neutrinos [37,38] in addition to supernova neutrinos [28].

There are two crucial differences between detecting supernova neutrinos in paleo detectors and in Hyper-Kamiokande/DUNE: First, the geological timescales paleo detectors record neutrino-interactions over are many orders of magnitude longer than the (inverse) supernova rate of the Milky Way (2 – 3 per century [15–20]). Physically then, paleo detectors are sensitive to the mean supernova neutrino properties from many past core collapses, similar to the DSNB modulo different distances. When averaged over timescales much longer than a century, the supernova neutrino flux on Earth is no longer dominated by the DSNB, but by neutrinos from supernovae in our galaxy, and this time-averaged flux is a factor of order 100 larger than the DSNB flux [28]. Second, paleo detectors would detect supernova neutrinos via coherent elastic neutrino-nucleus scattering (CEνNS), a process mediated by neutral currents and hence sensitive to the total neutrino flux rather than the $\bar{\nu}_e/\nu_e$ fluxes Hyper-Kamiokande/DUNE would measure. In this regard, paleo detectors utilize the same interaction physics as direct dark matter experiments. Combined with the significantly larger time-integrated galactic supernova neutrino flux, paleo detectors offer a unique opportunity to measure all flavors of neutrinos emitted from a population of past core-collapse events.

In order to extract the ν_x flux parameters, a measurement of the total galactic supernova neutrino flux in paleo detectors must be combined with flavor-sensitive measurements of supernova neutrinos. To this end, we consider a combination of the paleo-detector measurement with measurements of the DSNB $\bar{\nu}_e/\nu_e$ parameters with Hyper-Kamiokande/DUNE. The main background for supernova neutrinos in paleo detectors stems from radiogenic neutrons originating from the ^{238}U decay chain, and we project the precision to which the ν_x flux parameters can be extracted for different assumptions on the uranium concentration in paleo-detector samples. We find that for a ^{238}U concentration of 10^{-11} g/g (10^{-12} g/g), the average energy as well as the total energy of the ν_x flux can be measured with few tens of percent ($\lesssim$10%) precision.

The remainder of this work is structured as follows: In Sec. II, we discuss the calculation of the time-averaged flux of neutrinos from galactic supernovae at Earth, the calculation of the DSNB and the calculation of the neutrino-induced signal in paleo detectors. A discussion of the most relevant background sources in paleo detectors can be found in Sec. II A. In Sec. III we explain the statistical analysis we use to extract the neutrino parameters from mock data in Hyper-Kamiokande, DUNE, and paleo detectors. We show our results for the projected precision of the reconstruction of these parameters in Sec. IV. In Sec. V, we summarize and discuss our findings.

II. PALEO DETECTORS AS (SUPERNOVA) NEUTRINO DETECTORS

In this section, we discuss the signal from supernova neutrinos in paleo detectors as well as the most relevant backgrounds. For a more detailed discussion of paleo detectors as (CEνNS) neutrino detectors, see Ref. [28], and for discussions of the relevant background sources in paleo detectors see also Refs. [26,27].

We model the spectrum of the neutrino species ν_i from a supernova as a pinched Fermi-Dirac distribution [39]

$$\left(\frac{dn}{dE}\right)_{\nu_i} = E_\nu^{\mathrm{tot}} \frac{(1+\alpha)^{1+\alpha}}{\Gamma(1+\alpha)} \frac{E^\alpha}{\langle E_\nu \rangle^{2+\alpha}} e^{\left[-(1+\alpha)\frac{E}{\langle E_\nu \rangle}\right]}, \quad (1)$$

where E_ν^{tot} is the total energy radiated in ν_i, $\langle E_\nu \rangle$ is the average energy of the neutrinos, and α is a (dimensionless) spectral shape parameter. For flavor-blind interactions such as CEνNS, the relevant neutrino flux is the sum over all flavors,

$$\frac{dn}{dE_\nu} = \left(\frac{dn}{dE}\right)_{\nu_e} + \left(\frac{dn}{dE}\right)_{\bar{\nu}_e} + 4\left(\frac{dn}{dE}\right)_{\nu_x}. \tag{2}$$

The time-averaged neutrino spectrum from core-collapse supernovae in our Galaxy is then obtained by integrating over the probability density $f(R_E)$ for a supernova to occur at a distance R_E from Earth and by multiplying with the galactic core-collapse supernova rate, $\dot{N}_{\rm CC}^{\rm gal}$,

$$\left(\frac{d\phi}{dE_\nu}\right)^{\rm gal} = \dot{N}_{\rm CC}^{\rm gal}\frac{dn}{dE_\nu}\int_0^\infty dR_E \frac{f(R_E)}{4\pi R_E^2}. \tag{3}$$

For $f(R_E)$ we assume that supernovae occur predominantly in the stellar disk and model the distribution of core-collapse supernovae as a double-exponential in galactocentric coordinates,

$$\rho \propto e^{-R/R_d} e^{-|z|/H}, \tag{4}$$

where R is the galactocentric radius, z the height above the galactic plane, and we use $R_d = 2.9$ kpc and $H = 95$ pc [20].

Similarly, the DSNB neutrino flux is obtained by integrating over the volumetric cosmic supernova rate, $\dot{n}_{\rm CC}^{\rm cosmo}$, [21,22]

$$\left(\frac{d\phi}{dE_\nu}\right)^{\rm DSNB} = \int_0^\infty \frac{dz}{H_0\sqrt{\Omega_\Lambda + \Omega_m(1+z)^3}}\dot{n}_{\rm CC}^{\rm cosmo}(z)\frac{dn}{dE'_\nu}, \tag{5}$$

where $H_0 \simeq 67$ km/s/Mpc is the Hubble constant, $\Omega_\Lambda \simeq 0.68$ and $\Omega_m \simeq 0.32$ are the cosmological density parameters for dark energy and matter, respectively, and z is the cosmological redshift. Note that the supernova neutrino spectrum, dn/dE_ν, must be evaluated at the redshifted neutrino energy $E'_\nu = (1+z)E_\nu$. The cosmic supernova rate is related to the (volumetric) star formation rate $\dot{\rho}_*(z)$ via the conversion factor

$$\dot{n}_{\rm CC}^{\rm cosmo}(z) = \dot{\rho}_*(z)\frac{\int_{M_{\rm min}=8}^{100}\psi(M)dM}{\int_{0.1}^{100}M\psi(M)dM}, \tag{6}$$

which is equivalent to assuming that all massive stars with mass above $M_{\rm min} = 8\ M_\odot$ undergo core collapse. This is a reasonable assumption for our estimates (see, e.g., discussions in [40])—although a fraction of massive stars are expected to collapse to black holes, with systematically higher temperature neutrino emissions [41], we neglect their contribution in this work. First, their occurrence rate remains highly uncertain, and secondly, their contributions would enhance the detectability of the DSNB so we remain conservative by omitting their occurrence. The star-formation rate is observationally measured [42,43], especially well in the low redshift range of importance for estimating the DSNB, and we adopt the functional fit described in, e.g., Refs. [41,44]. Note that alternatively one could also take $\dot{n}_{\rm CC}^{\rm cosmo}(z)$ directly from supernova surveys, see for example Ref. [45]. However, the limited depth of current supernova surveys means that in the most relevant redshift range, $z \lesssim 2$, the errors of such direct measurements of $\dot{n}_{\rm CC}^{\rm cosmo}(z)$ are larger than those of inferring $\dot{n}_{\rm CC}^{\rm cosmo}(z)$ from measurements of the cosmic star formation rate via Eq. (6).

Supernova neutrinos (predominantly[1]) induce signals in paleo detectors via CEνNS interactions. The differential recoil spectrum (per unit target mass) for a target nucleus T to recoil with energy E_R is given by [46,47]

$$\left(\frac{dR}{dE_R}\right)_T = \frac{1}{m_T}\int_{E_\nu^{\rm min}} dE_\nu \frac{d\sigma}{dE_R}\frac{d\phi}{dE_\nu}, \tag{7}$$

where m_T is the mass of T and $E_\nu^{\rm min} = \sqrt{m_T E_R/2}$ is the minimum neutrino required to induce a nuclear recoil with E_R. The differential CEνNS cross section is

$$\frac{d\sigma}{dE_R}(E_R, E_\nu) = \frac{G_F^2}{4\pi}Q_W^2 m_T\left(1 - \frac{m_T E_R}{2E_\nu^2}\right)F^2(E_R), \tag{8}$$

with the Fermi coupling constant G_F, the nuclear form factor $F(E_R)$,[2] and

$$Q_W \equiv (A_T - Z_T) - (1 - 4\sin^2\theta_W)Z_T, \tag{9}$$

where θ_W is the weak mixing angle, and A_T (Z_T) the number of nucleons (protons) in T.

The observable in a paleo detector is the track length spectrum, which is obtained from the recoil energy spectrum by summing over all target nuclei and weighting with the stopping power of T in the material, dE_R/dx_T,

$$\frac{dR}{dx} = \sum_T \xi_T \frac{dE_R}{dx_T}\left(\frac{dR}{dE_R}\right)_T, \tag{10}$$

where ξ_T is the mass fraction of T in the target material. Similarly, the length x of a track from a nucleus T recoiling with energy E_R is obtained by integrating the stopping power,

$$x(E_R) = \int_0^{E_R} dE \left|\frac{dE}{dx_T}\right|^{-1}. \tag{11}$$

We use SRIM [49,50] to calculate stopping powers in the target materials used in this work, epsomite

[1]Additional signals arise via quasielastic charged-current interactions and, for more energetic neutrinos, via (deep) inelastic neutrino-nucleus interactions [36]. However, the contribution from quasielastic interactions is suppressed compared to the CEνNS one by the lack of coherent enhancement, and the contribution of inelastic interactions of more energetic neutrinos is suppressed by the quickly falling neutrino flux.

[2]We use the Helm form factor [48] as in Ref. [28].

$[Mg(SO_4)\cdot 7(H_2O)]$, gypsum $[Ca(SO_4)\cdot 2(H_2O)]$, and sinjarite $[CaCl_2\cdot 2(H_2O)]$.

A. Background sources

Let us briefly discuss the most relevant background sources for supernova neutrino searches in paleo detectors. These backgrounds have been discussed in detail in Refs. [26,28] see also Ref. [27]. Note that all relevant backgrounds stem from nuclear recoils. Natural defects in minerals are either single-site or span across the entire monocrystalline volume, and thus do not resemble the damage tracks induced by CEνNS of supernova neutrinos.

(i) *Cosmogenics*: In order to suppress cosmic-ray induced backgrounds, minerals used as paleo detectors must have been shielded by a sufficiently large overburden for the entire time they have been recording nuclear damage tracks. The modest amounts of target materials required for paleo detectors, at most a few kg, can be sourced from much greater depths than those of existing underground laboratories. For example, boreholes drilled for geological R&D or oil exploration are promising sources of samples. For an overburden of $\gtrsim$5 km rock, cosmogenic backgrounds, in particular the cosmogenic muon induced neutron flux, are suppressed to a negligible level.

(ii) *Radiogenics*: Any mineral used as a paleo detector will be contaminated by trace amounts of radioactive material. In order to mitigate the associated radiogenic backgrounds, it is crucial to use as radiopure minerals as possible as paleo detectors. The most important radioactive isotope in natural minerals is ^{238}U. Minerals formed in the Earth's crust have typical ^{238}U concentrations of $C^{238}\sim 10^{-6}$ g/g, which would lead to prohibitively large radiogenic backgrounds. The ^{238}U concentration in so-called ultra basic rocks (UBRs), formed from the material of the Earth's mantle, and in marine evaporites (MEs), salts formed from sea water, are much lower, making them attractive as paleo detectors, see Refs. [51–57] as well as the discussion in Refs. [26,28]. As in previous work on paleo detectors [25–28,36,58], we will assume benchmark ^{238}U concentrations of $C^{238}=10^{-11}$ g/g for the ME examples epsomite $[Mg(SO_4)\cdot 7(H_2O)]$, gypsum $[Ca(SO_4)\cdot 2(H_2O)]$, and sinjarite $[CaCl_2\cdot 2(H_2O)]$ we use as target materials in this work. We will also show prospects for measuring supernova neutrinos for a more optimistic assumption of $C^{238}=10^{-12}$ g/g. The most relevant radiogenic background in paleo detectors are nuclear recoils induced by the elastic scattering of radiogenic neutrons off the nuclei constituting the mineral. These neutrons are produced by spontaneous fission of heavy radiogenic isotopes as well as by (α,n)-reactions of the α-particles from the ^{238}U decay chain. We use `SOURCES-4A` [59] to model these neutron spectra, and calculate the induced nuclear recoil spectrum using `TENDL-2017` [60–63] neutron-nucleus cross sections as tabulated in the `JANIS4.0` database [64].[3]

(iii) *Astrophysical neutrinos*: Just like supernova neutrinos, neutrinos from other sources give rise to nuclear recoils and, in turn, nuclear damage tracks in paleo detectors. The most relevant backgrounds to supernova neutrino induced recoils are solar and atmospheric neutrinos. We take the corresponding neutrino fluxes from Ref. [68] and model the corresponding nuclear recoil spectrum as for the supernova neutrinos described above.

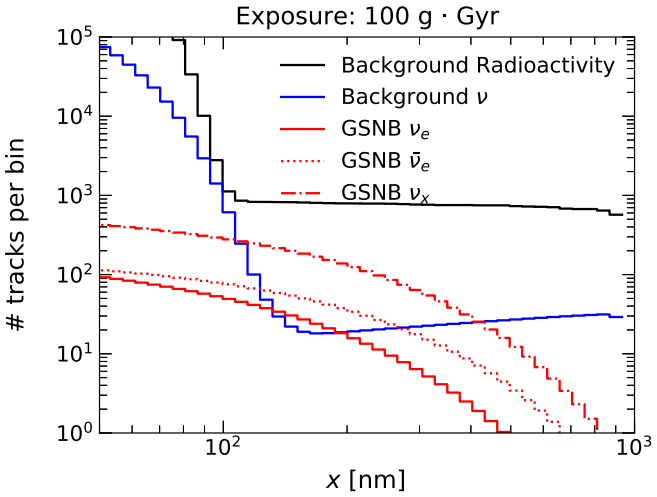

FIG. 1. Number of events per bins of track length in a Epsomite $[Mg(SO_4)\cdot 7(H_2O)]$ paleo detector with 100 gram Gyr exposure. Throughout this work, we use 70 log-spaced bins in the range 7.5 nm $\leq x \leq 10^3$ nm. The red lines show the events induced by CEνNS of neutrinos from core-collapse supernovae in our galaxy. The blue line indicates the spectrum induced by scattering of solar, atmospheric, and DSNB neutrinos, and the black line shows the spectrum induced by radiogenic neutrons. As we show in this work, by utilizing the entire spectrum the galactic supernova signal and its properties can be measured although it produces fewer tracks than the backgrounds for all track lengths.

In Fig. 1 we show the signal induced by the coherent scattering of neutrinos from supernovae in our Galaxy in

[3]We take only elastic neutron-nucleus scattering into account; this yields a conservative estimate of the background because neutrons typically lose a larger fraction of their energies through inelastic processes than in elastic scattering. Note also that our Monte Carlo simulation of the nuclear recoils induced by radiogenic neutrons has been validated with a calculation of the nuclear recoils induced by the same neutron spectra with `FLUKA` [65–67] in Ref. [36] for the particular case of a halite target.

epsomite [$Mg(SO_4)\cdot 7(H_2O)$] together with the backgrounds induced by other astrophysical neutrinos and radiogenic neutrons, assuming $C^{238} = 10^{-11}$ g/g. Note that we have included contributions from solar and atmospheric neutrinos as well as from the DSNB in the spectrum labeled "ν bkg." As we will see, the properties of the galactic supernova neutrino flux can be inferred in a paleo detector despite the fact that the overall normalization of the associated track length spectrum is smaller than that of the backgrounds. This is possible thanks to the enormous exposure achievable in paleo detectors: Reading out 100 g of a mineral which has been recording damage tracks for 1 Gyr corresponds to an exposure of $\varepsilon = 100\,\mathrm{g\,Gyr} = 100\,\mathrm{kt\,yr}$. For such an exposure, there would be about 2.8×10^3 ν_x tracks with length between 100 and 500 nm. In the same range, there would be 1.8×10^5 tracks from background events for our fiducial assumption of $C^{238} = 10^{-11}$ g/g. Therefore, considering only statistical uncertainty, the ν_x signal can be observed with a statistical significance of $2.8\times 10^3/\sqrt{1.8\times 10^5} = 6.6\sigma$. For the same exposure in gypsum [$Ca(SO_4)\cdot 2(H_2O)$] and sinjarite [$CaCl_2\cdot 2(H_2O)$], there would be a significance of 3σ and 2σ, respectively. Note that even for ^{238}U concentrations as large as $C^{238} = 5\times 10^{-11}$ g/g, the (statistical) significance for seeing ν_x induced tracks in an epsomite paleo detector would still be 3σ.

III. ANALYSIS

In order to calculate the track length distributions in paleo detectors for both supernova neutrino and background events we use the public code presented in Ref. [27]. In our analysis we employ three rock samples: Epsomite [$Mg(SO_4)\cdot 7(H_2O)$], gypsum [$Ca(SO_4)\cdot 2(H_2O)$] and sinjarite [$CaCl_2\cdot 2(H_2O)$]; these minerals provide particularly good detection statistics for supernova neutrinos. We assume that 100 g of each material can be read out with track length resolution of 15 nm.[4] Such a sample size and readout resolution may, for example, be achievable with small angle x-ray scattering microscopy [33–35], see the discussion in Ref. [26]. We consider both a default ^{238}U concentration of $C^{238} = 10^{-11}$ g/g and a more optimistic one of $C^{238} = 10^{-12}$ g/g. These choices are summarized in Table I. Concerning the neutrino energy spectrum, the parameters used for generating our set of mock data are given in Table II. These have been extracted from Fig. 1 in [69], where the first 3D supernova simulation up to 7 seconds post bounce has been presented, providing a more reliable estimate of the total energies of each neutrino species. In particular, the values for the average energies reported in Table II refer to the time-averaged quantities reported in Fig. 1 of [69], whereas the total energies are obtained by integrating over time.

TABLE I. Summary of paleo detector properties used in our simulation.

Track Resolution	15 nm
Track Length Min	7.5 nm
Track Length Max	1000 nm
Number of Log Bins	70
Rock Sample Mass	100 g
Rock Sample Age	1 Gyr
Default Uranium Concentration (C^{238})	10^{-11} g/g
Optimistic Uranium Concentration (C^{238})	10^{-12} g/g

Since the contribution of galactic supernova neutrinos to the track length distribution is subdominant with respect to the radiogenic and solar neutrino background, paleo detectors alone cannot (completely) break the degeneracy between the three supernova neutrino components ($\nu_e, \bar{\nu}_e, \nu_x$). To alleviate this problem we include an independent measurement of the DSNB with the future neutrino detectors DUNE [7,70–72] and Hyper-Kamiokande [6], which will be sensitive to ν_e and $\bar{\nu}_e$, respectively. Let us note that observations of the neutrinos from a single future galactic supernova in neutrino and dark matter detectors can, in general, provide much higher precision measurements of the supernova neutrino spectrum than the combined measurement of the DSNB in DUNE and Hyper-Kamiokande and galactic supernova neutrinos in paleo detectors we consider here. However, our approach has two important advantages. First, we do not need to wait for the next galactic core-collapse supernova. Second, our approach would measure neutrinos from a large population of supernovae rather than from one specific (possibly atypical) supernova.

TABLE II. Summary of neutrino properties used to generate our set of mock data. Note that $E^{\mathrm{tot}}_{\nu_x}$ refers to the total energy of one of the four ν_x neutrino species ($\nu_\mu, \bar{\nu}_\mu, \nu_\tau, \bar{\nu}_\tau$), see Eq. (2), and α_ν is the pinching-parameter of the energy distribution of neutrinos [39], see Eq. (1).

$\langle E_{\nu_e}\rangle$	11.2 MeV
$\langle E_{\bar{\nu}_e}\rangle$	13.5 MeV
$\langle E_{\nu_x}\rangle$	13.4 MeV
$E^{\mathrm{tot}}_{\nu_e}$	6.8×10^{52} erg
$E^{\mathrm{tot}}_{\bar{\nu}_e}$	6.6×10^{52} erg
$E^{\mathrm{tot}}_{\nu_x}$	6.2×10^{52} erg
$\alpha_{\nu_e} = \alpha_{\nu_x} = \alpha_{\bar{\nu}_e}$	3
Galactic Supernova Rate	0.023 per year

[4] In order to include the effects of finite track length resolution, we compute the number of tracks in the ith bin with reconstructed length $x \in [x_i^{\min}, x_i^{\max}]$ in a sample of mass M which has been recording tracks for a time t_{age} as $N_i = M\times t_{\mathrm{age}}\int dx' W(x'; x_i^{\min}, x_i^{\max})(dR/dx')$, where dR/dx' is the true track length spectrum and W is a window function, see, for example, Ref. [27].

In order to project the precision with which DUNE and Hyper-Kamiokande can constrain the parameters controlling the supernova neutrino spectrum, we compute the DSNB flux as in Eq. (5), except that we use the spectrum from the appropriate single neutrino flavor ν_i rather than the total neutrino flux, see Eqs. (1) and (2). For detection at DUNE, we consider a 40 kton liquid argon detector and detection of electron neutrinos through the charged-current interaction $\nu_e + \mathrm{Ar} \to e^- + \mathrm{K}^+$. We adopt the cross section based on the random phase approximation scheme of Ref. [73]. Since DUNE is under construction, we assume a detection efficiency of 86% based on the DUNE design report [7,74]. For detection at Hyper-Kamiokande, we consider a gadolinium-enhanced water detector with fiducial volume of 187 kton and detection of antielectron neutrinos through inverse-beta interaction on water $\bar{\nu}_2 + p \to n + e^+$. The cross section is well-known [75,76], and we assume a detection efficiency of 67% [74]. For detector backgrounds, we consider the models adopted in Refs. [74,77]. These include for Hyper-Kamiokande atmospheric neutrinos, spallation products, and invisible muons (i.e., tracks produced by the decay products of sub-Cherenkov threshold muons); and for DUNE, atmospheric neutrinos. We consider a 20-year run time for both Hyper-Kamiokande and DUNE. We note that although other detectors, e.g., JUNO [78], have sensitivity to DSNB neutrinos [77], DUNE and Hyper-Kamiokande will dominate the sensitivity to ν_e and $\bar{\nu}_e$, respectively.

In our analysis we perform a scan over a 12-dimensional parameter space. Six parameters correspond to the average and total energies of $\nu_e, \bar{\nu}_e$ and ν_x (the pinching parameters α_{ν_i} are fixed to the values in Table II). The floating parameters related to paleo detectors are the normalization of the radiogenic and solar neutrino background. Those related to DSNB measurements are the normalization of the backgrounds in DUNE and Hyper-Kamiokande, for which we adopt the spectra modeled in Refs. [74,77]. The last two parameters are the galactic supernova rate and the overall normalization of the DSNB signal, which parametrize the uncertainty on the star formation rate. We introduce Gaussian priors with (relative) width of 10% on the galactic supernova rate and the normalization of the DSNB, and priors with 20% width on the background normalization in DUNE and Hyper-Kamiokande. To put our choices of priors on the galactic supernova rate and the DSNB in context, we note that the uncertainty on the cosmic star formation rate is already at the level of ∼20% at the low redshifts most relevant to the DSNB and local core collapses [21,42,43]. We expect considerable improvements on this uncertainty in the next decade, not least from the upcoming surveys with the James Webb Space Telescope [79] and the Vera C. Rubin Observatory [80]. While the time evolution of the galactic star formation rate on gigayear timescales remains uncertain with tens-of-percent fluctuations (see, e.g., Refs. [81–83]), we emphasize that the relevant quantity for our analysis is the local supernova rate integrated over the past ∼1 Gy rather than the instantaneous rate. Note that we are not including any priors on the normalization of the solar neutrino and radiogenic backgrounds in paleo detectors nor on the total and mean energies of the supernova neutrino fluxes. We scan over the parameter space using a Markov Chain Monte Carlo through the public software PyMultinest [84,85]. We define the following likelihood:

$$\begin{aligned}\log(\mathcal{L}) = &-\sum_{i=1}^{N_{\mathrm{bins}}^{\mathrm{paleo}}}[N_i^{\mathrm{th}} - N_i^{\mathrm{data}} + N_i^{\mathrm{data}}(\log(N_i^{\mathrm{data}}) \\ &- \log(N_i^{\mathrm{th}})] - \frac{1}{2}\sum_p \left(\frac{f_p}{\sigma_p}\right)^2 \\ &- \sum_{\mathrm{exp}}\sum_{i=1}^{N_{\mathrm{bins}}^{\mathrm{exp}}}[M_{\mathrm{exp},i}^{\mathrm{th}} - M_{\mathrm{exp},i}^{\mathrm{data}} \\ &+ M_{\mathrm{exp},i}^{\mathrm{data}}(\log(M_{\mathrm{exp},i}^{\mathrm{data}}) - \log(M_{\mathrm{exp},i}^{\mathrm{th}})], \end{aligned} \tag{12}$$

where N_i^{data} is the number of simulated data events in the ith track length bin for paleo detectors and N_i^{th} the number of expected events, defined as $N_i^{\mathrm{th}} = N_i^{0,\mathrm{th}}(1 + \sum_p f_p)$, where the f_p are the free normalization parameters discussed above and $N_i^{0,\mathrm{th}}$ is the expected number of events calculated with the default values of parameters. $M_{\mathrm{exp},i}^{\mathrm{data,th}}$ is defined analogously to N_i^{th}, but refers to DSNB events for exp = (Hyper-Kamiokande, DUNE). Concerning the binning, we use 70 log-spaced bins between 7.5 nm and 10^3 nm.

For the DSNB we take into account also possible neutrino oscillations inside the supernova.[5] In particular, focusing only on the MSW effect and neglecting collective and turbulence effects, we consider three cases: no oscillations, normal and inverted mass ordering. For normal mass ordering the survival probability of ν_e is $P(\nu_e \to \nu_e) = 0$, whereas the one for $\bar{\nu}_e$ is $P(\bar{\nu}_e \to \bar{\nu}_e) = 0.7$. For inverted mass ordering the survival probability of ν_e is $P(\nu_e \to \nu_e) = 0.3$, whereas the one for $\bar{\nu}_e$ is $P(\bar{\nu}_e \to \bar{\nu}_e) = 0$. Note that when we report our projected constraints on the neutrino parameters below, neutrino flavors always refer to the those emitted in the supernova explosion, i.e., prior to any flavor oscillations.

IV. RESULTS

Figure 2 displays the allowed regions at 68% and 99.7% confidence levels for the average energy and total energy of each neutrino flavor obtained when using only the measurement of DSNB neutrinos in DUNE and

[5]Since paleo detectors measure supernova neutrinos (predominantly) via CEνNS, flavor oscillations have no effect on the signal in paleo detectors.

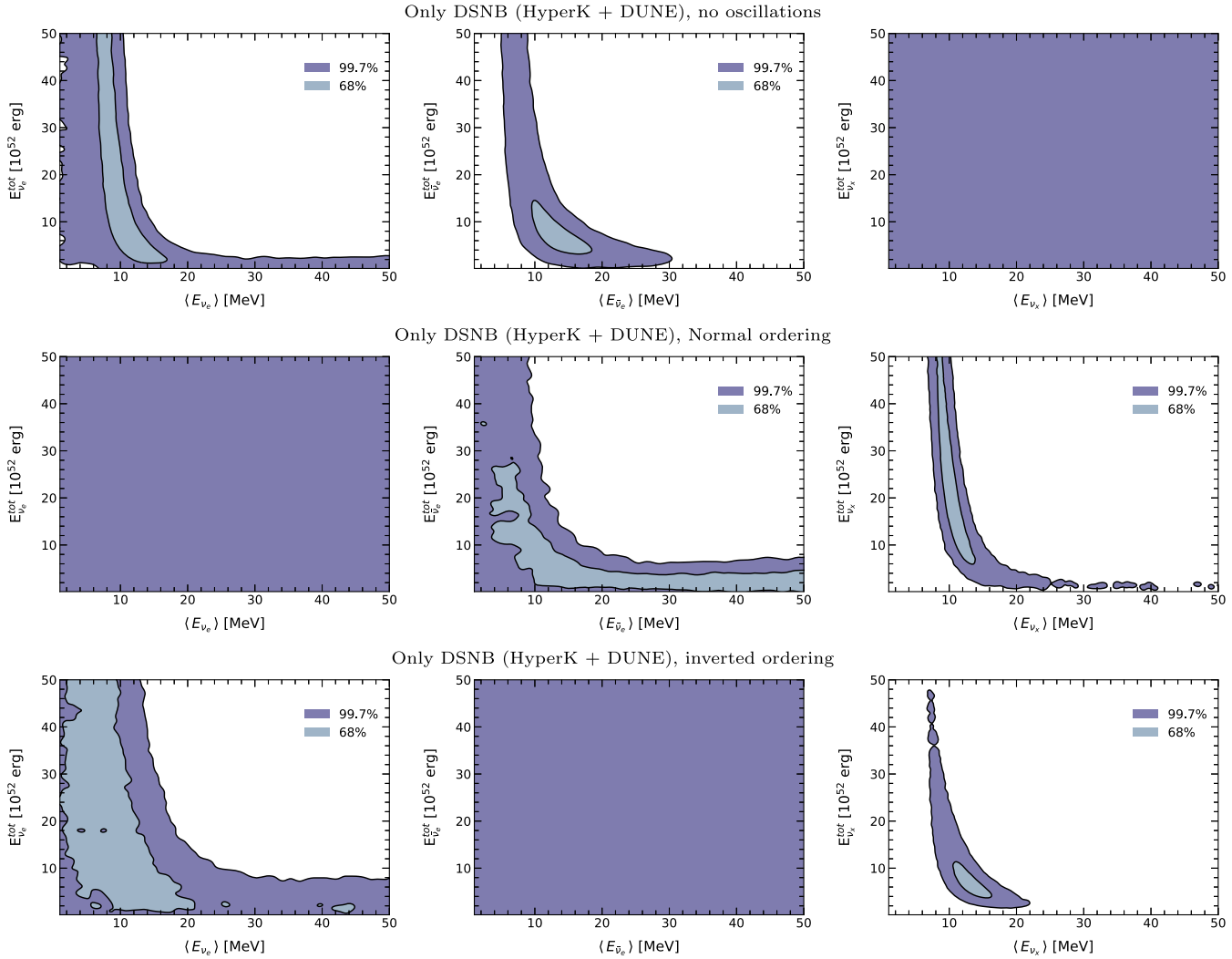

FIG. 2. Posterior probability distribution function of the supernova neutrino parameters obtained by observing the DSNB in DUNE and Hyper-Kamiokande only. The left column shows the projection in the plane of the ν_e average energy vs total energy, the middle column shows the $\bar{\nu}_e$ flavor, and the right column for the ν_x flavor parameters. The panels in the top row are for the "no oscillation" scenario, while the middle (bottom) row shows results for normal (inverted) ordering. Note that for "no oscillation"/normal ordering/ inverted ordering, DUNE and Hyper-Kamiokande alone do not constrain the $\nu_x/\nu_e/\bar{\nu}_e$ parameters.

Hyper-Kamiokande for 20-years of operation, i.e., the results in Fig. 2 are without any information one could obtain from measuring the galactic supernova neutrino flux in paleo detectors. In all figures presented in this section, the left panels show the projection in the plane of the ν_e average energy vs total energy, the middle panels are for the $\bar{\nu}_e$ flavor parameters, and the right panels for the ν_x flavor parameters; the panels in the top row are for the "no oscillation" scenario, while the middle (bottom) row shows results for normal (inverted) ordering. In general, a degeneracy between average energy and total energy is observed, which is due to the fact that the statistics of the signal events is proportional to the product $\langle E_{\nu_\alpha} \rangle^2 E^{\rm tot}_{\nu_\alpha}$.

Let us discuss the results for the different oscillation scenarios in a little more detail: For the "no oscillation" case (shown in the top row), we find slightly better precision for the $\bar{\nu}_e$ parameters (middle panel) than for the ν_e parameters (left panel). This is due to the better statistics of the $\bar{\nu}_e$ events in Hyper-Kamiokande compared to the ν_e events in DUNE. Since under the assumptions made in this work neither Hyper-Kamiokande nor DUNE are sensitive to ν_x neutrinos, we do not find any corresponding constraint in the top right panel.

For the normal ordering case shown in the middle row, recall that the survival probability for ν_e is $P(\nu_e \to \nu_e) = 0$ and for $\bar{\nu}_e$, $P(\bar{\nu}_e \to \bar{\nu}_e) = 0.7$. Accordingly, we find no constraint for the ν_e parameters, while the constraint for the $\bar{\nu}_e$ parameters is somewhat worse than for the "no oscillation" case. On the other hand, ν_x produced in the supernovae now oscillate into ν_e and $\bar{\nu}_e$ at the detector,

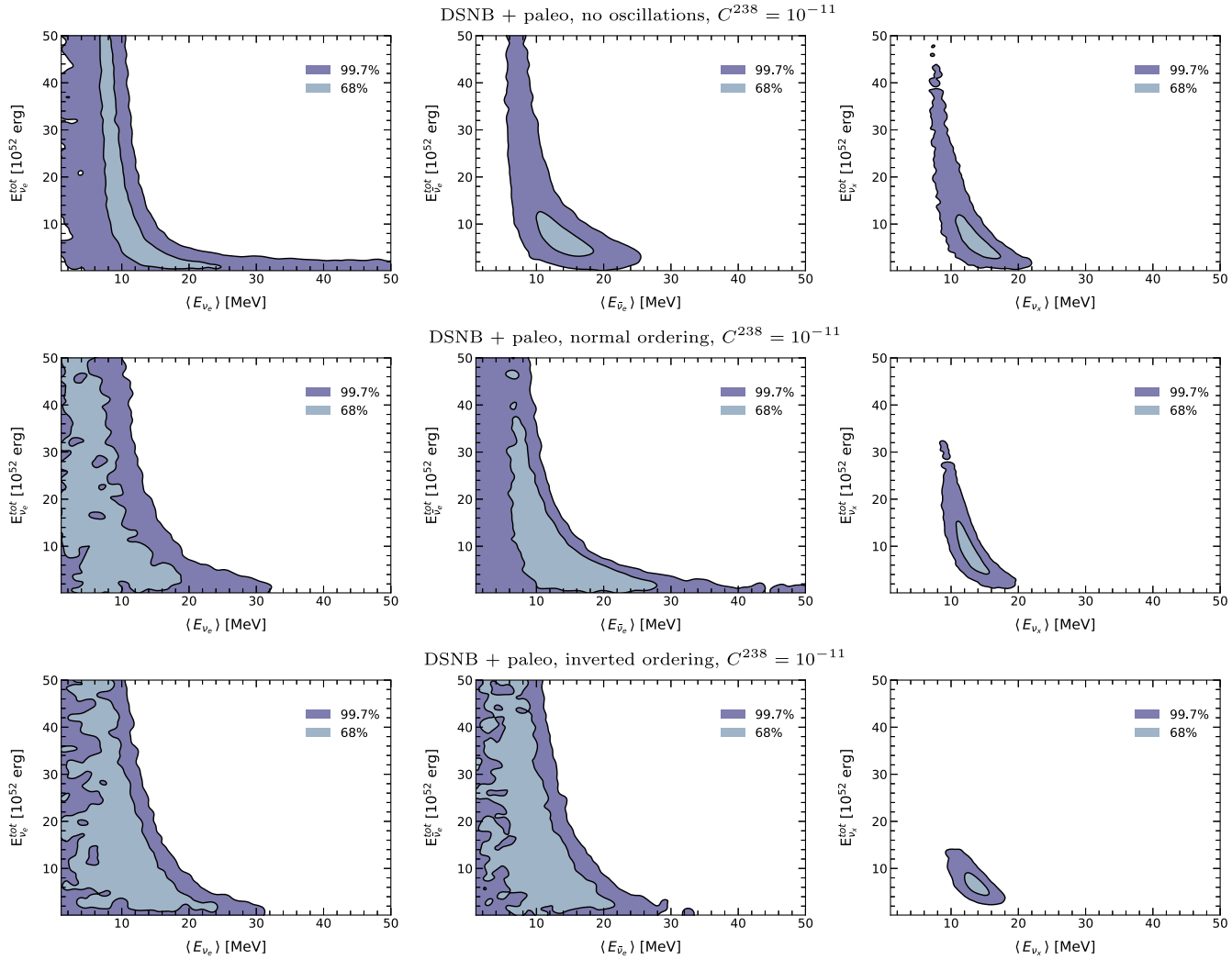

FIG. 3. Posterior probability distribution functions of the supernova neutrino parameters obtained when combining DSNB observations in DUNE and Hyper-Kamiokande with paleo detector observations of the galactic supernova neutrino flux, assuming $C^{238} = 10^{-11}$. As in Fig. 2, the left, central and right columns refer to ν_e $\bar{\nu}_e$ and ν_x, respectively, whereas from top to bottom the rows of panels refer to the case of no oscillations, normal ordering and inverted ordering, respectively. The addition of the flavor-blind measurement in paleo detector allows sensitivity to all flavors under all oscillation scenarios considered here.

hence, we find a constraint of the ν_x parameters from Hyper-Kamiokande and DUNE alone.

For the inverted ordering case [where $P(\nu_e \to \nu_e) = 0.3$ and $P(\bar{\nu}_e \to \bar{\nu}_e) = 0$] shown in the bottom row, the posterior probability distribution functions change compare to the "no oscillation" case for analogous reasons: In this scenario, one obtains no constraint on the $\bar{\nu}_e$ parameters and the constraints on the ν_e parameters degrade compared to the "no oscillation" scenario. As in the normal ordering case, one does obtain a constraint on the ν_x parameters for inverted ordering, and the allowed regions for the ν_x parameters are somewhat smaller for inverted ordering than for normal ordering due to the oscillation patterns and the different detection statistics of $\bar{\nu}_e$ in Hyper-Kamiokande vs ν_e in DUNE.

Figure 3 displays the allowed regions at 68 and 99.7% confidence levels for the average energy and total energy of ν_e, $\bar{\nu}_e$ and ν_x obtained by using both the information obtainable with a paleo-detector measurement of galactic supernova neutrinos and the DSNB in Hyper-Kamiokande and DUNE. Here, we have assumed a uranium concentration of $C^{238} = 10^{-11}$ g/g, controlling the normalization of the most important background for the supernova neutrino measurement with paleo detectors. Compared to the Hyper-Kamiokande+DUNE only results shown in Fig. 2, adding the information of the flavor-blind measurement in paleo detectors now allows to obtain constraints on all neutrino flavors regardless of the oscillation parameters. Note that since $\nu_x = \{\nu_\mu, \bar{\nu}_\mu, \nu_\tau, \bar{\nu}_\tau\}$ contribute roughly four times more to the total neutrino

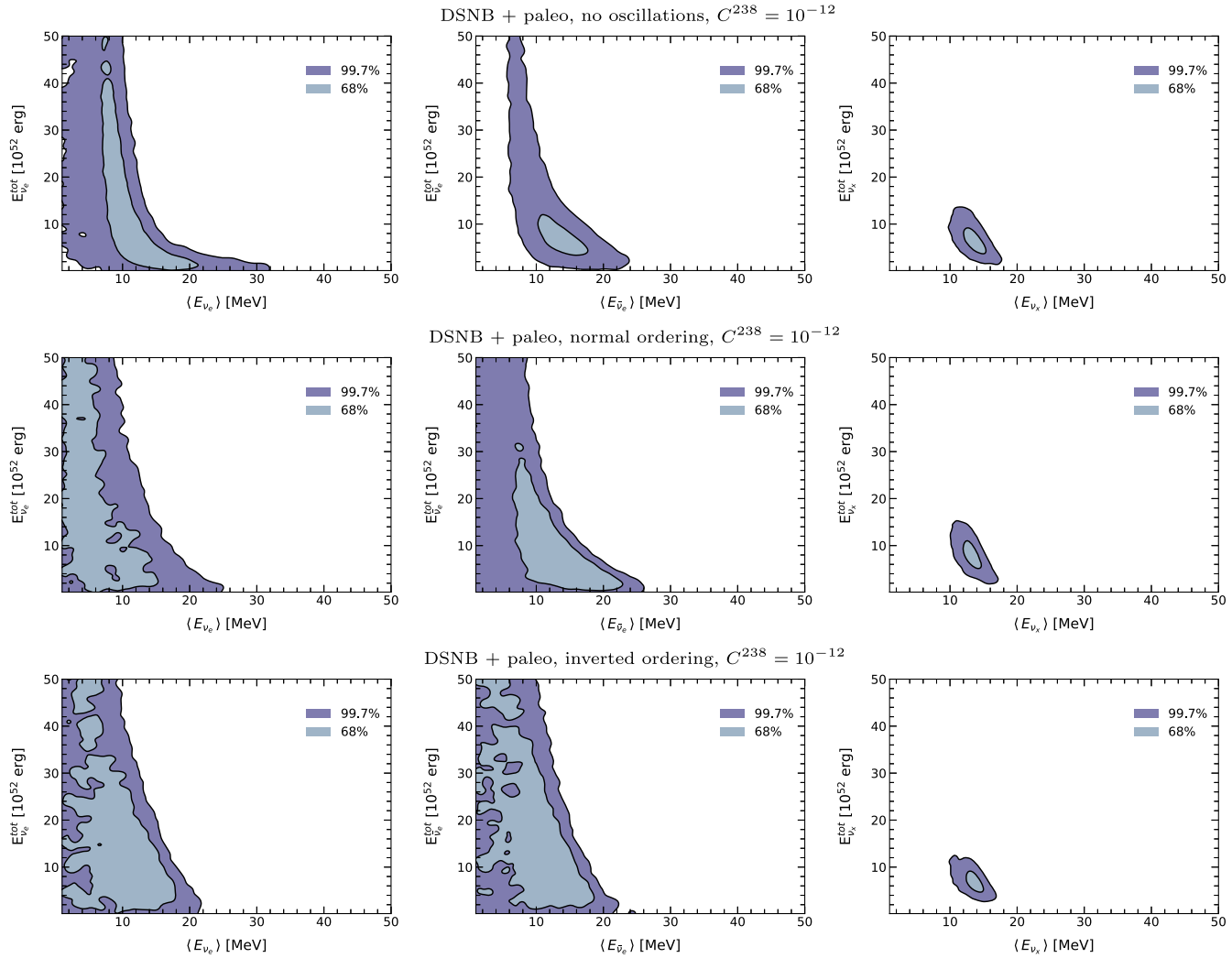

FIG. 4. Same as Fig. 3, except that we assume $C^{238} = 10^{-12}$. Left, central and right columns refer to ν_e $\bar{\nu}_e$ and ν_x, respectively, whereas from top to bottom the rows refer to the case of no oscillations, normal ordering and inverted ordering, respectively.

flux than ν_e or $\bar{\nu}_e$, see Eq. (2), the signal in paleo detectors alone is dominated by ν_x. Nonetheless, in combination with information from the DSNB measurements in Hyper-Kamiokande and DUNE, paleo detectors also improved the measurements of the ν_e and $\bar{\nu}_e$ parameters. For the no-oscillation case, where all the information on the ν_x parameters stems from paleo detectors, we find that the values $E^{\rm tot}_{\nu_x} = 0$ and $\langle E_{\nu_x} \rangle = 0$ are disfavored at more than 99.7% confidence level. For both normal and inverted ordering, shown in the middle and bottom rows of Fig. 3, respectively, the bounds on ν_x parameters are slightly improved with respect to the no oscillation case. Recall that although oscillations do not affect the neutral current coherent scattering signal in paleo detectors, oscillations do lead to signals from the ν_x component in either Hyper-Kamiokande or DUNE, depending on the mass ordering under consideration. The best precision on the ν_x parameters is reached for inverted ordering, since in this case, ν_x can be observed in Hyper-Kamiokande, which has a larger statistics compared to DUNE.

In Fig. 4 we show the projected constraints on the supernova neutrino parameters for the three different assumptions of the flavor oscillations considered above but for a more optimistic ^{238}U concentration of $C^{238} = 10^{-12}$ g/g in the paleo detectors rather than the $C^{238} = 10^{-11}$ g/g assumed in Fig. 3. Comparing these figures we can see that using paleo detectors with uranium concentration of $C^{238} = 10^{-12}$ g/g would allow us to constrain $\langle E_{\nu_x} \rangle$ and $E^{\rm tot}_{\nu_x}$ with (relative) precision $\lesssim$10% rather than the few tens of percent precision we project for $C^{238} = 10^{-11}$ g/g. This improvement is due to the reduction of the dominant background in paleo detectors, the (elastic) scattering of neutrons originating from the ^{238}U decay chain.

If we modify the assumption of a 10% prior on both the galactic supernova rate and the normalization of the DSNB,

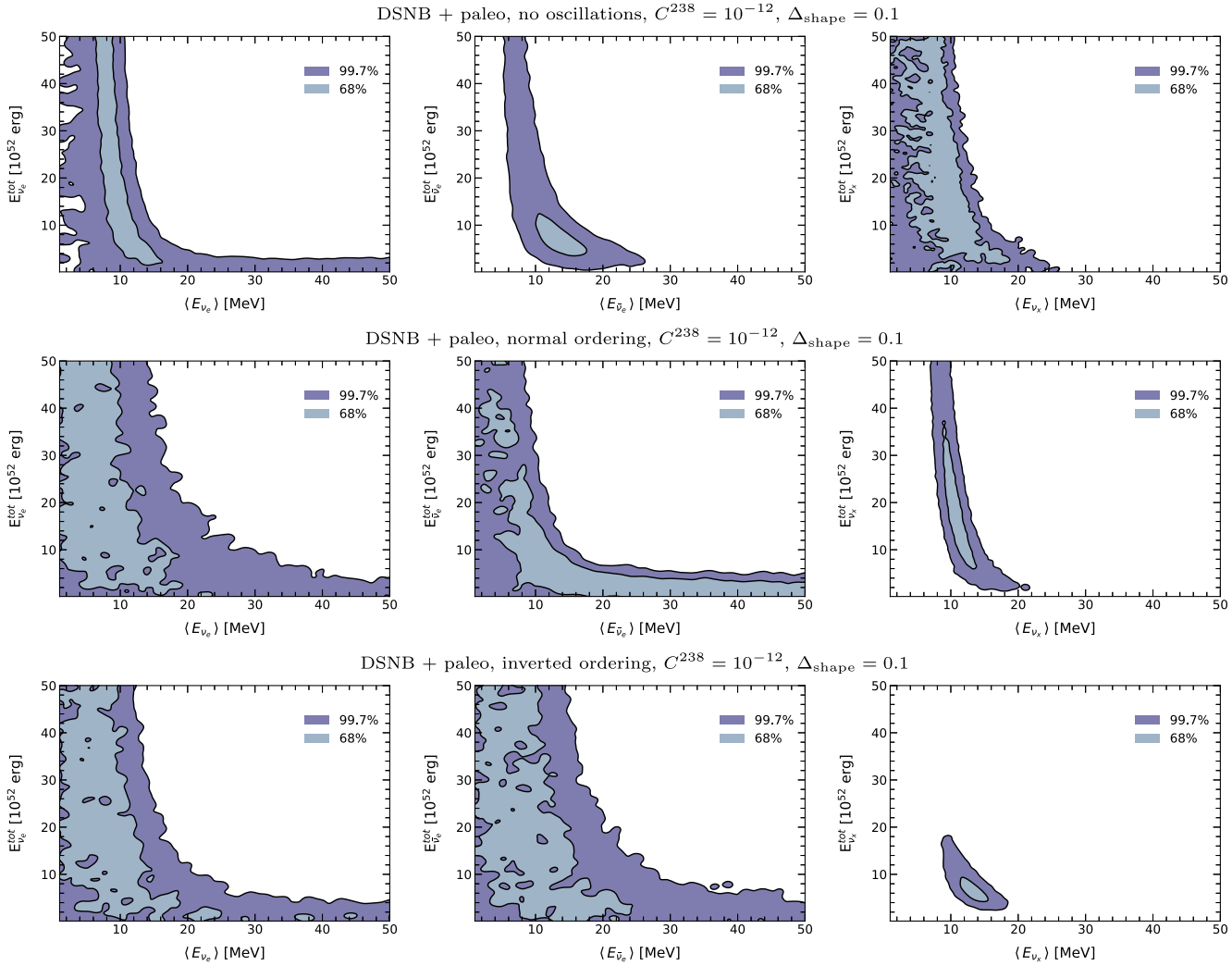

FIG. 5. Same as Fig. 4 but with uncorrelated shape uncertainties as parametrized in Eq. (13), with $\Delta_{\rm shape} = 0.1$. Left, central and right columns refer to ν_e $\bar{\nu}_e$ and ν_x, respectively, whereas from top to bottom the rows refer to the case of no oscillations, normal ordering and inverted ordering, respectively.

our results are significantly affected (not shown). In particular, when increasing the width of these priors to 20%, the 99.7% confidence level region extends toward $\langle E_{\nu_x} \rangle = 0$ and large values of $E^{\nu_x}_{\rm tot}$. This happens because widening this prior loosens the link between the DSNB measurements in Hyper-Kamiokande and DUNE with the paleo-detector measurement of neutrinos from galactic core-collapse events, making it possible for the contribution of ν_x to be compensated by ν_e and $\bar{\nu}_e$. On the other hand, increasing the uncertainty on the normalization of backgrounds for DSNB experiments does not appreciably affect the final constraints on $\langle E_{\nu_x} \rangle$ and $E^{\rm tot}_{\nu_x}$.

The sensitivity shown so far can be strongly affected when considering uncertainties in the shape of signal and background spectra in paleo detectors beyond simple normalization factors. To take these into account we follow Ref. [27] and we substitute the first term in Eq. (12) with

$$\log(\mathcal{L}) \supset -\frac{1}{2}\sum_{i=1}^{N^{\rm paleo}_{\rm bins}} \frac{(N_i^{\rm th} - N_i^{\rm data})^2}{N_i^{\rm data} + (\Delta_{\rm shape} N_i^{\rm data})^2}. \quad (13)$$

This is a conservative choice, because the term $(\Delta_{\rm shape} N_i^{\rm data})^2$ represents uncertainties uncorrelated among bins, which cannot be further constrained in the fit. These can be considered as a combination of uncertainties of each component of the track length distribution, for which our partial ignorance on the corresponding shape cannot be parametrized with an analytical formula. The results of the analysis, taking $\Delta_{\rm shape} = 0.1$, is shown in Fig. 5. Note that the choice of $\Delta_{\rm shape} = 0.1$ here is not based on any specific systematic consideration, but is where we start to see a significant deterioration in the ability to constrain supernova neutrino parameters. The results are strongly dependent on the oscillation scenario under consideration.

Without oscillations, all the information on ν_x comes from paleo detectors, which cannot measure the corresponding flux with a precision better than the uncertainties set by the term $(\Delta_{\rm shape} N_i^{\rm data})^2$. With normal ordering and inverted ordering we have an increasingly precise external input from DUNE and HyperK, respectively. In particular, for inverted ordering we almost recover the nominal allowed regions reported in Fig. 4.

The precision with which the supernova neutrino parameters can be inferred can also be reduced if the track length resolution in paleo detectors is worse than what we assumed above. With a doubled and quadrupled width of the resolution (not shown) the precision degrades mostly in the case of no oscillation and normal ordering, while it stays nearly unchanged in inverted ordering. The reason for this oscillation dependence is analogous to what happens in the case of shape uncertainties.

A final remark is in order. Recently, the possibility of measuring the DSNB in conventional dark matter detectors and extracting the ν_x parameters has been carefully studied in Ref. [24]. Analogously to the signal in paleo detectors, in conventional dark matter detectors the supernova neutrino signal is dominated by background, but the signal-to-noise ratio is smaller for two reasons: Conventional dark matter detectors have much smaller exposures than paleo detectors (e.g., the DARWIN proposal has an envisaged exposure on the order of $\varepsilon \sim 100\,\mathrm{t\,yr}$ [23]). Second, conventional dark matter detectors would be sensitive to DSNB neutrinos, while paleo detectors could measure the (time-averaged) signal from galactic supernova neutrinos; the time-averaged galactic supernova flux is roughly two orders of magnitude larger than the DNSB flux. This difference in the signal-to-noise ratio is the reason why in Ref. [24], only prospective upper limits on ν_x parameters are provided, whereas in our work, we show goodness-of–fit regions. Nevertheless, the two approaches to measure the ν_x component are complementary. Paleo detectors allow only to probe galactic supernovae, whereas dark matter detectors can measure the DSNB, which includes extragalactic supernova neutrinos. Furthermore, neutrinos propagating over cosmological distances, like those of the DSNB, allow studying different fundamental physics (see, for example, Refs. [86,87]).

V. CONCLUSIONS

Supernova neutrinos carry invaluable information about the astrophysical processes occurring deep inside a stellar core collapse. The few tens of events observed from SN1987a have already demonstrated the potential of detecting a supernova neutrino burst, despite the small statistics collected. Next generation experiments, such as Hyper-Kamiokande, DUNE and JUNO, would detect $\mathcal{O}(10^5)\bar{\nu}_e$, $\mathcal{O}(10^3)\nu_e$ and $\mathcal{O}(10^2)\nu_x$ events, respectively, from a galactic supernova, thus covering all neutrino flavors with differing precision. However, only a few supernovae are expected to occur per century in our galaxy on average, and the only remedy is patience. A possible way around this problem is probing the DSNB, i.e., the integrated flux of neutrinos produced by all the supernova explosions occurring throughout the Universe. Another benefit of the DSNB is that it allows one to be sensitive to the entire population of supernovae and not only to a specific progenitor, which might have peculiar characteristics. Hyper-Kamiokande, DUNE and JUNO have the capability to detect the DSNB, but with much smaller statistics compared to a single galactic supernova and with a significant background to deal with. For $\bar{\nu}_e$ events in Hyper-Kamiokande, such background can be mitigated by adding gadolinium in the water Cherenkov detector, which can provide a 90% efficiency in tagging inverse beta decay events induced by neutrinos. For ν_x, the detection prospects are less promising, even considering dark matter detectors where the background is intrinsically lower. For instance, the expected number of DSNB events in XENONnT is $\mathcal{O}(10^{-3})$ per year [24], whereas the background is expected to add up to a few events per year [88]. In this case only upper limits can be set on the parameters describing the ν_x flux, i.e., the average energy and total energy, $\langle E_{\nu_x}\rangle$ and $E_{\nu_x}^{\rm tot}$ [24].

In this work we have shown that one could *measure* the ν_x parameters using paleo detectors. Differently from conventional detectors which measure neutrino events in real time, paleo detectors integrate events over timescales as large as a billion years. Thus, paleo detectors could measure the integrated neutrino flux from core-collapse supernovae in our Galaxy via the nuclear recoils induced by (flavor-blind) CEνNS reactions of neutrinos with the atomic nuclei in paleo detectors. Leveraging the gigayear exposure times, with only 100 g of a epsomite paleo detector, we expect about 3×10^3 ν_x events and a background of 2×10^5 events, assuming a uranium-238 concentration of $C^{238} = 10^{-11}$ g/g. Although the signal-to-background ratio is similar to what is expected for DSNB events in dark matter detectors, the statistics is orders of magnitude higher, leading to a much better signal-to-noise ratio—the ratio between signal events and the square root of background is 6.6σ. Combining such a measurement of the galactic supernova neutrino flux with measurements of the DSNB via charged current interactions in Hyper-Kamiokande and DUNE would allow to provide closed contours of the 68% and 99.7% confidence level regions for the parameters controlling the supernova neutrino spectra of all flavors, ν_e, $\bar{\nu}_e$, and ν_x. With a more optimistic assumption on the concentration of uranium, $C^{238} = 10^{-12}$ g/g, we project that the parameters $\langle E_{\nu_x}\rangle$ and $E_{\nu_x}^{\rm tot}$ could be measured with a precision of $\lesssim$10% on

each parameters. However, the precision on some of these supernova neutrino parameters can be lost for uncertainties on the DSNB and galactic supnernova rate larger than the 10% assumed here. Current uncertainties on the cosmic star formation rate at low redshifts are already at the level of ∼20% [21,42,43], and while reaching ∼10% uncertainties is ambitious, upcoming surveys with, for example, the James Webb Space Telescope or the Vera C. Rubin Observatory are expected to lead to considerable improvements in our knowledge of the cosmic and local star formation rate in the near future. We emphasize that the use of paleo detectors is complementary to the one of dark matter detectors, since they are sensitive to a different population of supernova progenitors and potentially to different effects of physics beyond the Standard Model.

ACKNOWLEDGMENTS

S. B. is supported in part by NSF Grant No. PHY-2014215, DOE HEP QuantISED Award No. 100495, and the Gordon and Betty Moore Foundation Grant No. GBMF7946. The work of F. C. at Virginia Tech is supported by the U.S. Department of Energy under the Awards No. DE-SC0020250 and No. DE-SC0020262. The work of F. C. at I. F. I. C. is supported by GVA Grant No. CDEIGENT/2020/003. The work of S. H. is supported by the U.S. Department of Energy under the Award No. DE-SC0020262 and NSF Grants No. AST-1908960 and No. PHY-1914409. This work was supported by World Premier International Research Center Initiative (WPI Initiative), MEXT, Japan. This research was supported in part by the National Science Foundation under Grant No. NSF PHY-1748958. S. H. was also supported by NSF Grant No. PHY-2209420 and JSPS KAKENHI Grant No. JP22K03630.

[1] K. Hirata *et al.* (Kamiokande-II Collaboration), Observation of a Neutrino Burst from the Supernova SN 1987a, Phys. Rev. Lett. **58**, 1490 (1987).
[2] R. M. Bionta *et al.*, Observation of a Neutrino Burst in Coincidence with Supernova SN 1987a in the Large Magellanic Cloud, Phys. Rev. Lett. **58**, 1494 (1987).
[3] M. Aglietta *et al.*, Supernova 1987A in the Large Magellanic Cloud, IAU Circular No. 4323 (1987).
[4] E. N. Alekseev, L. N. Alekseeva, I. V. Krivosheina, and V. I. Volchenko, Detection of the neutrino signal from SN1987A in the LMC using the INR Baksan underground scintillation telescope, Phys. Lett. B **205**, 209 (1988).
[5] S. Horiuchi and J. P. Kneller, What can be learned from a future supernova neutrino detection?, J. Phys. G **45**, 043002 (2018).
[6] K. Abe *et al.* (Hyper-Kamiokande Collaboration), Hyper-Kamiokande design report, arXiv:1805.04163.
[7] B. Abi *et al.* (DUNE Collaboration), Deep underground neutrino experiment (DUNE), Far detector technical design report, volume II: DUNE physics, arXiv:2002.03005.
[8] J. F. Beacom, W. M. Farr, and P. Vogel, Detection of supernova neutrinos by neutrino proton elastic scattering, Phys. Rev. D **66**, 033001 (2002).
[9] B. Dasgupta and J. F. Beacom, Reconstruction of supernova ν_μ, ν_τ, anti-ν_μ, and anti-ν_τ neutrino spectra at scintillator detectors, Phys. Rev. D **83**, 113006 (2011).
[10] H.-L. Li, Y.-F. Li, M. Wang, L.-J. Wen, and S. Zhou, Towards a complete reconstruction of supernova neutrino spectra in future large liquid-scintillator detectors, Phys. Rev. D **97**, 063014 (2018).
[11] H.-L. Li, X. Huang, Y.-F. Li, L.-J. Wen, and S. Zhou, Model-independent approach to the reconstruction of multi-flavor supernova neutrino energy spectra, Phys. Rev. D **99**, 123009 (2019).
[12] B. Chauhan, B. Dasgupta, and V. Datar, A deuterated liquid scintillator for supernova neutrino detection, J. Cosmol. Astropart. Phys. 11 (2021) 005.
[13] C. J. Horowitz, K. J. Coakley, and D. N. McKinsey, Supernova observation via neutrino-nucleus elastic scattering in the CLEAN detector, Phys. Rev. D **68**, 023005 (2003).
[14] R. F. Lang, C. McCabe, S. Reichard, M. Selvi, and I. Tamborra, Supernova neutrino physics with xenon dark matter detectors: A timely perspective, Phys. Rev. D **94**, 103009 (2016).
[15] E. Cappellaro, R. Barbon, and M. Turatto, Supernova statistics, Springer Proc. Phys. **99**, 347 (2005).
[16] R. Diehl *et al.*, Radioactive Al-26 and massive stars in the galaxy, Nature (London) **439**, 45 (2006).
[17] A. Strumia and F. Vissani, Neutrino masses and mixings and…, arXiv:hep-ph/0606054.
[18] W. Li, R. Chornock, J. Leaman, A. V. Filippenko, D. Poznanski, X. Wang, M. Ganeshalingam, and F. Mannucci, Nearby supernova rates from the Lick Observatory Supernova Search—III. The rate-size relation, and the rates as a function of galaxy Hubble type and colour, Mon. Not. R. Astron. Soc. **412**, 1473 (2011).
[19] M. T. Botticella, S. J. Smartt, R. C. Kennicutt, Jr., E. Cappellaro, M. Sereno, and J. C. Lee, A comparison between star formation rate diagnostics and rate of core collapse supernovae within 11 Mpc, Astron. Astrophys. **537**, A132 (2012).
[20] S. M. Adams, C. S. Kochanek, J. F. Beacom, M. R. Vagins, and K. Z. Stanek, Observing the next galactic supernova, Astrophys. J. **778**, 164 (2013).
[21] J. F. Beacom, The diffuse supernova neutrino background, Annu. Rev. Nucl. Part. Sci. **60**, 439 (2010).
[22] C. Lunardini, Diffuse supernova neutrinos at underground laboratories, Astropart. Phys. **79**, 49 (2016).

[23] J. Aalbers *et al.* (DARWIN Collaboration), DARWIN: Towards the ultimate dark matter detector, J. Cosmol. Astropart. Phys. 11 (2016) 017.
[24] A. M. Suliga, J. F. Beacom, and I. Tamborra, Towards probing the diffuse supernova neutrino background in all flavors, Phys. Rev. D **105**, 043008 (2022).
[25] S. Baum, A. K. Drukier, K. Freese, M. Górski, and P. Stengel, Searching for dark matter with paleo-detectors, Phys. Lett. B **803**, 135325 (2020).
[26] A. K. Drukier, S. Baum, K. Freese, M. Górski, and P. Stengel, Paleo-detectors: Searching for dark matter with ancient minerals, Phys. Rev. D **99**, 043014 (2019).
[27] S. Baum, T. D. P. Edwards, K. Freese, and P. Stengel, New projections for dark matter searches with paleo-detectors, Instruments **5**, 21 (2021).
[28] S. Baum, T. D. P. Edwards, B. J. Kavanagh, P. Stengel, A. K. Drukier, K. Freese, M. Górski, and C. Weniger, Paleodetectors for galactic supernova neutrinos, Phys. Rev. D **101**, 103017 (2020).
[29] R. L. Fleischer, P. B. Price, R. M. Walker, and E. L. Hubbard, Track registration in various solid-state nuclear track detectors, Phys. Rev. **133**, A1443 (1964).
[30] R. L. Fleischer, P. B. Price, and R. M. Walker, Tracks of charged particles in solids, Science **149**, 383 (1965).
[31] R. L. Fleischer, P. B. Price, and R. M. Walker, Solid-state track detectors: Applications to nuclear science and geophysics, Annu. Rev. Nucl. Part. Sci. **15**, 1 (1965).
[32] S.-L. Guo, B.-L. Chen, and S. Durrani, Chapter 4—solid-state nuclear track detectors, in *Handbook of Radioactivity Analysis (Third Edition)*, edited by M. F. L'Annunziata (Academic Press, Amsterdam, 2012), pp. 233–298, 10.1016/B978-0-12-384873-4.00004-9.
[33] M. Rodriguez, W. Li, F. Chen, C. Trautmann, T. Bierschenk, B. Afra, D. Schauries, R. Ewing, S. Mudie, and P. Kluth, Saxs and tem investigation of ion tracks in neodymium-doped yttrium aluminium garnet, Nucl. Instrum. Methods Phys. Res., Sect. A **326**, 150 (2014).
[34] F. Schaff, M. Bech, P. Zaslansky, C. Jud, M. Liebi, M. Guizar-Sicairos, and F. Pfeiffer, Six-dimensional real and reciprocal space small-angle x-ray scattering tomography, Nature (London) **527**, 353 (2015).
[35] M. Holler, A. Diaz, M. Guizar-Sicairos, P. Karvinen, E. Färm, E. Härkönen, M. Ritala, A. Menzel, J. Raabe, and O. Bunk, X-ray ptychographic computed tomography at 16 nm isotropic 3d resolution, Sci. Rep. **4**, 3857 (2014).
[36] J. R. Jordan, S. Baum, P. Stengel, A. Ferrari, M. C. Morone, P. Sala, and J. Spitz, Measuring Changes in the Atmospheric Neutrino Rate Over Gigayear Timescales, Phys. Rev. Lett. **125**, 231802 (2020).
[37] J. I. Collar, Comments on 'Limits on Dark Matter Using Ancient Mica', Phys. Rev. Lett. **76**, 331 (1996).
[38] N. Tapia-Arellano and S. Horiuchi, Measuring solar neutrinos over gigayear timescales with paleo detectors, Phys. Rev. D **103**, 123016 (2021).
[39] M. T. Keil, G. G. Raffelt, and H.-T. Janka, Monte Carlo study of supernova neutrino spectra formation, Astrophys. J. **590**, 971 (2003).
[40] S. Horiuchi, J. F. Beacom, and E. Dwek, The diffuse supernova neutrino background is detectable in Super-Kamiokande, Phys. Rev. D **79**, 083013 (2009).
[41] S. Horiuchi, K. Sumiyoshi, K. Nakamura, T. Fischer, A. Summa, T. Takiwaki, H.-T. Janka, and K. Kotake, Diffuse supernova neutrino background from extensive core-collapse simulations of $8-100M_{\odot}$ progenitors, Mon. Not. R. Astron. Soc. **475**, 1363 (2018).
[42] A. M. Hopkins and J. F. Beacom, On the normalisation of the cosmic star formation history, Astrophys. J. **651**, 142 (2006).
[43] P. Madau and M. Dickinson, Cosmic star formation history, Annu. Rev. Astron. Astrophys. **52**, 415 (2014).
[44] S. Horiuchi, T. Kinugawa, T. Takiwaki, K. Takahashi, and K. Kotake, Impact of binary interactions on the diffuse supernova neutrino background, Phys. Rev. D **103**, 043003 (2021).
[45] L.-G. Strolger, T. Dahlen, S. A. Rodney, O. Graur, A. G. Riess, C. McCully, S. Ravindranath, B. Mobasher, and A. K. Shahady, The rate of core collapse supernovae to redshift 2.5 from The CANDELS and CLASH supernova Surveys, Astrophys. J. **813**, 93 (2015).
[46] J. Billard, L. Strigari, and E. Figueroa-Feliciano, Implication of neutrino backgrounds on the reach of next generation dark matter direct detection experiments, Phys. Rev. D **89**, 023524 (2014).
[47] C. A. J. O'Hare, Dark matter astrophysical uncertainties and the neutrino floor, Phys. Rev. D **94**, 063527 (2016).
[48] R. H. Helm, Inelastic and elastic scattering of 187-Mev electrons from selected even-even nuclei, Phys. Rev. **104**, 1466 (1956).
[49] J. F. Ziegler, J. P. Biersack, and U. Littmark, *The Stopping and Range of Ions in Solids* (Pergamon Press, New York, 1985).
[50] J. F. Ziegler, M. D. Ziegler, and J. P. Biersack, SRIM—The stopping and range of ions in matter (2010), Nucl. Instrum. Methods Phys. Res., Sect. B **268**, 1818 (2010).
[51] S. Thomson and G. Wardle, Coloured natural rocksalts: A study of their helium contents, colours and impurities, Geochim. Cosmochim. Acta **5**, 169 (1954).
[52] K. C. Condie, C. S. Kuo, R. M. Walker, and V. R. Murthy, Uranium distribution in separated clinopyroxenes from four eclogites, Science **165**, 57 (1969).
[53] J. A. S. Adams, J. K. Osmond, and J. J. W. Rogers, The geochemistry of thorium and uranium, Phys. Chem. Earth **3**, 298 (1959).
[54] M. Seitz and S. Hart, Uranium and boron distributions in some oceanic ultramafic rocks, Earth Planet. Sci. Lett. **21**, 97 (1973).
[55] W. E. Dean, Section V trace and minor elements in evaporites, in *Marine Evaporites* (SEPM Society for Sedimentary Geology, 1987), 10.2110/scn.78.01.0086.
[56] M. Yui, Y. Kikawada, T. Oi, T. Honda, and T. Nozaki, Abundance of uranium and thorium in rock salts, Radioisotopes **47**, 488 (1998).
[57] W. Sanford, M. Doughten, T. Coplen, A. Hunt, and T. Bullen, Evidence for high salinity of Early Cretaceous sea water from the Chesapeake Bay crater, Nature (London) **503**, 252 (2013).
[58] T. D. P. Edwards, B. J. Kavanagh, C. Weniger, S. Baum, A. K. Drukier, K. Freese, M. Górski, and P. Stengel, Digging for dark matter: Spectral analysis and discovery

potential of paleo-detectors, Phys. Rev. D **99**, 043541 (2019).
[59] D. G. Madland *et al.*, SOURCES 4A: A Code for Calculating (alpha,n), Spontaneous Fission, and Delayed Neutron Sources and Spectra, Technical Report No. LA-13639-MS, Los Alamos National Lab, 1999, 10.2172/15215.
[60] A. J. Koning and D. Rochman, Modern nuclear data evaluation with the TALYS code system, Nucl. Data Sheets **113**, 2841 (2012).
[61] D. Rochman, A. J. Koning, J. C. Sublet, M. Fleming *et al.*, The TENDL library: Hope, reality and future, in *Proceedings of the International Conference on Nuclear Data for Science and Technology, 2016, Bruges, Belgium*, 2016, https://tendl.web.psi.ch/bib_rochman/tendl.nd2016.pdf.
[62] J. C. Sublet, A. J. Koning, D. Rochman, M. Fleming, and M. Gilbert, TENDL-2015: Delivering both completeness and robustness, in Advances in Nuclear Nonproliferation Technology and Policy Conference, Santa Fe, NM, USA, https://tendl.web.psi.ch/bib_rochman/ANTPC_TENDL.pdf.
[63] M. Fleming, J. C. Sublet, J. Kopecky, D. Rochman, and A. J. Koning, Probing experimental and systematic trends of the neutron-induced TENDL-2014 nuclear data library, in CCFE report UKAEA-R(15)29, 2015 (2015), https://tendl.web.psi.ch/bib_rochman/UKAEA-R(15)29_30.9.15.pdf.
[64] N. Soppera, M. Bossant, and E. Dupont, JANIS 4: An improved version of the NEA java-based nuclear data information system, Nucl. Data Sheets **120**, 294 (2014).
[65] A. Ferrari, P. R. Sala, A. Fasso, and J. Ranft, FLUKA: A multi-particle transport code (Program version 2005), Reports No. CERN-2005-010, No. SLAC-R-773, No. INFN-TC-05-11.
[66] T. T. Böhlen, F. Cerutti, M. P. W. Chin, A. Fassò, A. Ferrari, P. G. Ortega, A. Mairani, P. R. Sala, G. Smirnov, and V. Vlachoudis, The FLUKA code: Developments and challenges for high energy and medical applications, Nucl. Data Sheets **120**, 211 (2014).
[67] G. Battistoni, A. Ferrari, M. Lantz, P. R. Sala, and G. I. Smirnov, A neutrino-nucleon interaction generator for the FLUKA Monte Carlo code, in *12th International Conference on Nuclear Reaction Mechanisms* (CERN-Proceedings-2010-001, Geneva, 2010), pp. 387–394.
[68] C. A. J. O'Hare, Can we overcome the neutrino floor at high masses?, Phys. Rev. D **102**, 063024 (2020).
[69] R. Bollig, N. Yadav, D. Kresse, H. T. Janka, B. Müller, and A. Heger, Self-consistent 3D supernova models from −7 minutes to +7 s: A 1-bethe explosion of a ∼19 $M_\odot$ progenitor, Astrophys. J. **915**, 28 (2021).
[70] B. Abi *et al.* (DUNE Collaboration), Deep underground neutrino experiment (DUNE), Far detector technical design report, volume I introduction to DUNE, J. Instrum. **15**, T08008 (2020).
[71] B. Abi *et al.* (DUNE Collaboration), Deep underground neutrino experiment (DUNE), Far detector technical design report, volume III: DUNE far detector technical coordination, J. Instrum. **15**, T08009 (2020).
[72] B. Abi *et al.* (DUNE Collaboration), Deep underground neutrino experiment (DUNE), Far detector technical design report, volume IV: Far detector single-phase technology, J. Instrum. **15**, T08010 (2020),
[73] E. Kolbe, K. Langanke, G. Martinez-Pinedo, and P. Vogel, Neutrino nucleus reactions and nuclear structure, J. Phys. G **29**, 2569 (2003).
[74] Z. Tabrizi and S. Horiuchi, Flavor triangle of the diffuse supernova neutrino background, J. Cosmol. Astropart. Phys. 05 (2021) 011.
[75] P. Vogel and J. F. Beacom, Angular distribution of neutron inverse beta decay, $\bar{\nu}_e + p e^+ + n$, Phys. Rev. D **60**, 053003 (1999).
[76] A. Strumia and F. Vissani, Precise quasielastic neutrino/nucleon cross-section, Phys. Lett. B **564**, 42 (2003).
[77] K. Møller, A. M. Suliga, I. Tamborra, and P. B. Denton, Measuring the supernova unknowns at the next-generation neutrino telescopes through the diffuse neutrino background, J. Cosmol. Astropart. Phys. 05 (2018) 066.
[78] Z. Djurcic *et al.* (JUNO Collaboration), JUNO conceptual design report, arXiv:1508.07166.
[79] J. P. Gardner *et al.*, The James webb space telescope, Space Sci. Rev. **123**, 485 (2006).
[80] P. A. Abell *et al.* (LSST Science Collaboration), LSST science book, Version 2.0, arXiv:0912.0201.
[81] O. Snaith, M. Haywood, P. Di Matteo, M. D. Lehnert, F. Combes, D. Katz, and A. Gómez, Reconstructing the star formation history of the Milky Way disc(s) from chemical abundances, Astron. Astrophys. **578**, A87 (2015).
[82] M. Haywood, M. D. Lehnert, P. Di Matteo, O. Snaith, M. Schultheis, D. Katz, and A. Gómez, When the Milky Way turned off the lights: APOGEE provides evidence of star formation quenching in our galaxy, Astron. Astrophys. **589**, A66 (2016).
[83] R. Mor, A. C. Robin, F. Figueras, S. Roca-Fabregas, and X. Luri, Gaia DR2 reveals a star formation burst in the disc 2–3 Gyr ago, Astron. Astrophys. **624**, L1 (2019).
[84] F. Feroz, M. P. Hobson, and M. Bridges, MultiNest: An efficient and robust Bayesian inference tool for cosmology and particle physics, Mon. Not. R. Astron. Soc. **398**, 1601 (2009).
[85] J. Buchner, A. Georgakakis, K. Nandra, L. Hsu, C. Rangel, M. Brightman, A. Merloni, M. Salvato, J. Donley, and D. Kocevski, X-ray spectral modelling of the AGN obscuring region in the CDFS: Bayesian model selection and catalogue, Astron. Astrophys. **564**, A125 (2014).
[86] Y. S. Jeong, S. Palomares-Ruiz, M. H. Reno, and I. Sarcevic, Probing secret interactions of eV-scale sterile neutrinos with the diffuse supernova neutrino background, J. Cosmol. Astropart. Phys. 06 (2018) 019.
[87] A. De Gouvêa, I. Martinez-Soler, Y. F. Perez-Gonzalez, and M. Sen, Fundamental physics with the diffuse supernova background neutrinos, Phys. Rev. D **102**, 123012 (2020).
[88] E. Aprile *et al.* (XENON Collaboration), Projected WIMP sensitivity of the XENONnT dark matter experiment, J. Cosmol. Astropart. Phys. 11 (2020) 031.